

Figure Captions

Fig. 1 Potential energy profiles and corresponding molecular structures for the $\text{LA} + \text{SO}_3 \rightarrow \text{LAS}$ reaction in the absence and presence of H_2O and H_2SO_4 investigated at the CCSD(T)-F12/cc-pVDZ-F12//M06-2X/6-311++G(2df,2pd) level

Fig. 2 (a) Effective rate constants for the $\text{LA} + \text{SO}_3 \rightarrow \text{LAS}$ reaction in the presence of H_2O (k'_{WM} , $\text{cm}^3 \cdot \text{molecule}^{-1} \cdot \text{s}^{-1}$) and H_2SO_4 (k'_{SA} , $\text{cm}^3 \cdot \text{molecule}^{-1} \cdot \text{s}^{-1}$) calculated using the master equation over the temperature range of 230-320 K; (b) Effective rate constants (k' , s^{-1}) for the hydrolysis of SO_3 with various species X ($X = \text{LA}, \text{SA}, \text{NA}, \text{FA}$ and OA) within the temperature range of 230-320 K, where SA, NA, FA and OA are denoted as H_2SO_4 , HNO_3 , HCOOH and $\text{H}_2\text{C}_2\text{O}_4$, respectively.

Fig. 3 Electrostatic potential (ESP)-mapped van der Waals surfaces of A, LAS and SA molecules. ESP minima and maxima for different functional groups are shown as blue and yellow spheres, respectively, with their corresponding values ($\text{kcal} \cdot \text{mol}^{-1}$) indicated in parentheses. Red arrows denote preferred directions for hydrogen bond formation, while blue arrows illustrate likely pathways for proton transfer.

Fig. 4 The total evaporation rates ($\sum \gamma$) (s^{-1}) of $(\text{SA})_x(\text{A})_y(\text{LAS})_z$ ($y \leq x + z \leq 3$) clusters at 278.15 K and 1 atm calculated at the M06-2X/6-311++G(2df, 2pd) level of theory. (a) without LAS monomer, (b) containing 1 LAS monomer, (c) containing 2 LAS monomers, and (d) containing 3 LAS monomers

Fig. 5 Nucleation mechanism of the LAS-SA-A system. (a) Cluster formation pathway at 278.15 K, with concentrations of $[\text{SA}] = 10^6$, $[\text{A}] = 10^9$ and $[\text{LAS}] = 10^5 \text{ molecules} \cdot \text{cm}^{-3}$; (b) the branch ratio of outward flux at different temperatures. Only net fluxes contributing more than 5% to cluster growth are depicted.

Fig. 6 Branching ratios of SA-A-LAS (red) and SA-A (blue) cluster growth pathways in regions with varying $[\text{LAS}]$ concentrations. Black data points indicate field observations, while blue points represent the median values used in this study. Ammonia concentration is fixed at $10^9 \text{ molecules} \cdot \text{cm}^{-3}$. Map source: ©Google Maps (<https://www.google.com/maps>)

Fig. 7 (a) Gibbs free energies ΔG ($\text{kcal} \cdot \text{mol}^{-1}$) and total evaporation rates $\sum \gamma$ (s^{-1}) for $(\text{LA})_x(\text{SA})_y(\text{A})_3$ and $(\text{LAS})_x(\text{SA})_y(\text{A})_3$ ($x = 0-3$, $x + y = 3$) clusters calculated at the M06-2X/6-311++G(2df, 2pd) level of theory and 278.15 K, (b) Cluster formation rate (J) and enhancement strength (R) for LAS as a function of monomer concentrations ($[\text{LA}]$ and $[\text{LAS}]$) at 278.15 K, with $[\text{SA}]$ fixed at $10^5 \text{ molecules} \cdot \text{cm}^{-3}$ and $[\text{A}]$ at $10^9 \text{ molecules} \cdot \text{cm}^{-3}$.

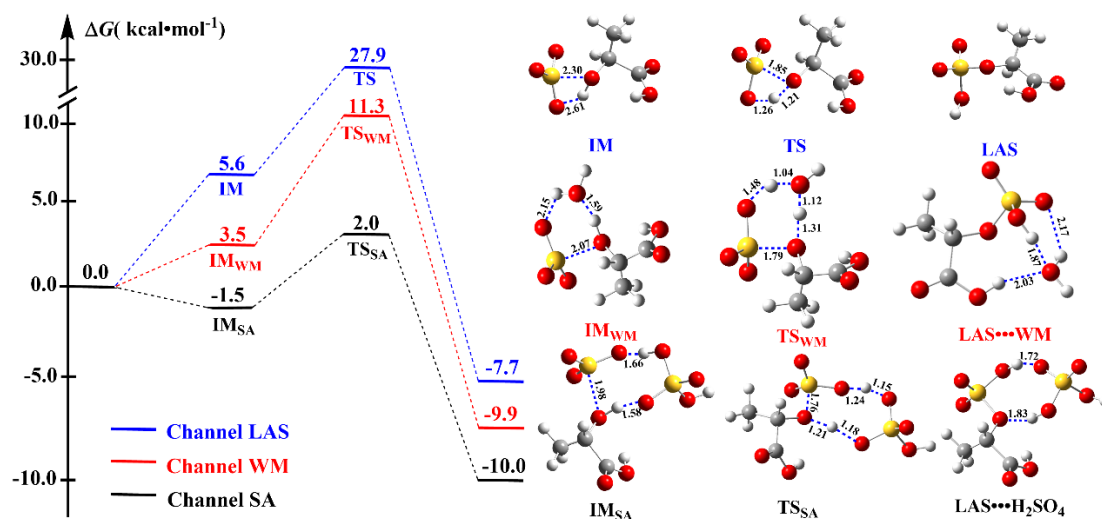


Fig. 1 Potential energy profiles and corresponding molecular structures for the $\text{LA} + \text{SO}_3 \rightarrow \text{LAS}$ reaction in the absence and presence of H_2O and H_2SO_4 investigated at the CCSD(T)-F12/cc-pVDZ-F12//M06-2X/6-311++G(2df,2pd) level

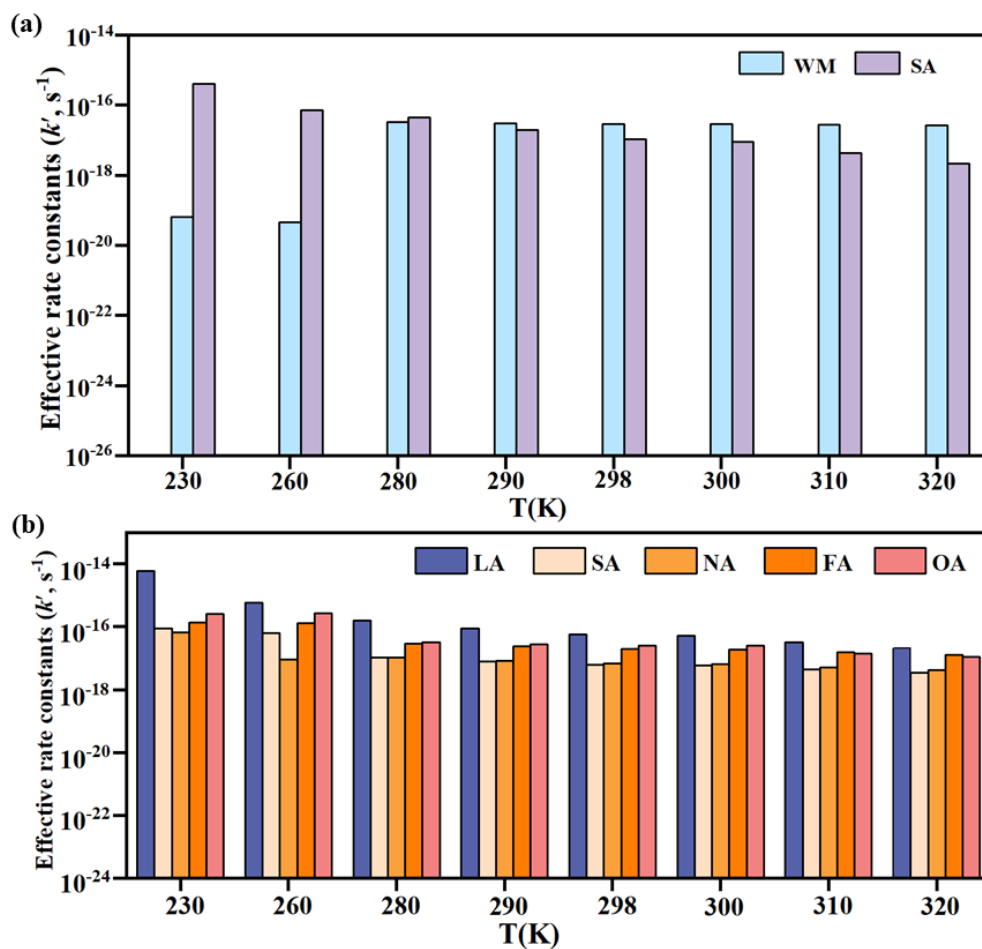


Fig. 2 (a) Effective rate constants for the $\text{LA} + \text{SO}_3 \rightarrow \text{LAS}$ reaction in the presence of H_2O (k'_{WM} , $\text{cm}^3 \cdot \text{molecule}^{-1} \cdot \text{s}^{-1}$) and H_2SO_4 (k'_{SA} , $\text{cm}^3 \cdot \text{molecule}^{-1} \cdot \text{s}^{-1}$) calculated using the master equation over the temperature range of 230-320 K; (b) Effective rate constants (k' , s^{-1}) for the hydrolysis of SO_3 with various species X ($X = \text{LA, SA, NA, FA}$ and OA) within the temperature range of 230-320 K, where SA, NA, FA and OA are denoted as H_2SO_4 , HNO_3 , HCOOH and $\text{H}_2\text{C}_2\text{O}_4$, respectively.

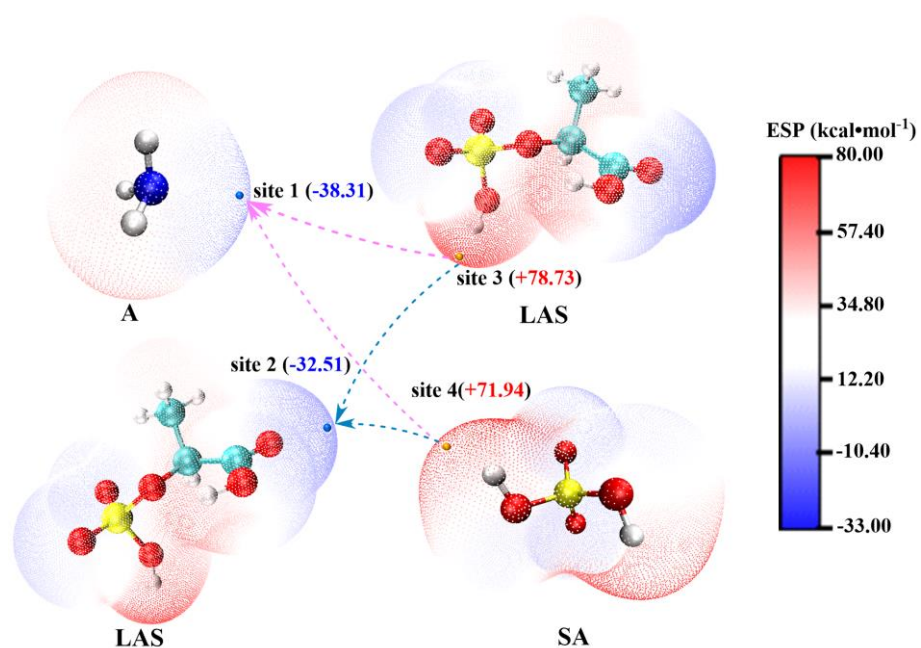


Fig. 3 Electrostatic potential (ESP)-mapped van der Waals surfaces of A, LAS and SA molecules. ESP minima and maxima for different functional groups are shown as blue and yellow spheres, respectively, with their corresponding values (kcal·mol⁻¹) indicated in parentheses. Red arrows denote preferred directions for hydrogen bond formation, while blue arrows illustrate likely pathways for proton transfer.

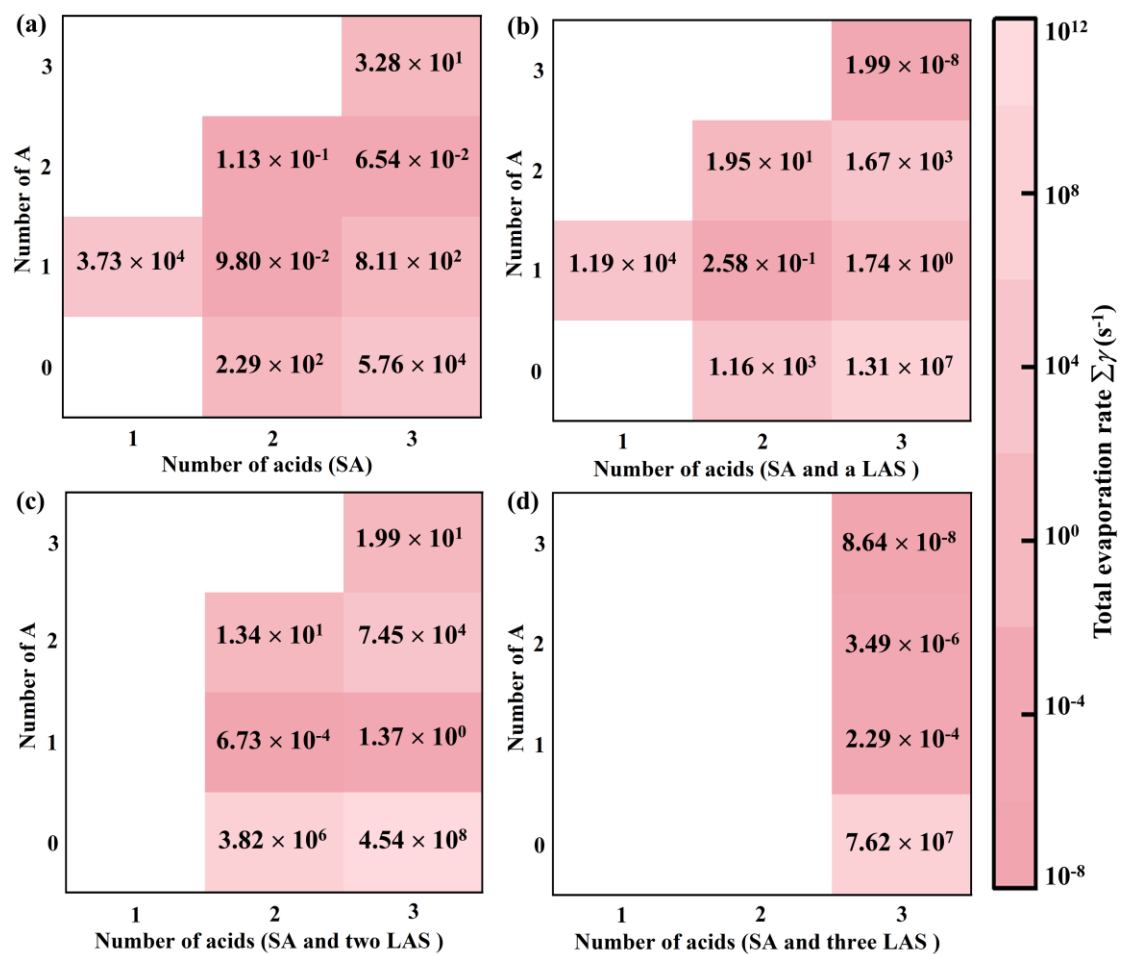


Fig. 4 The total evaporation rates ($\sum \gamma$) (s^{-1}) of $(\text{SA})_x(\text{A})_y(\text{LAS})_z$ ($y \leq x + z \leq 3$) clusters at 278.15 K and 1 atm calculated at the M06-2X/6-311++G(2df, 2pd) level of theory. (a) without LAS monomer, (b) containing 1 LAS monomer, (c) containing 2 LAS monomers, and (d) containing 3 LAS monomers

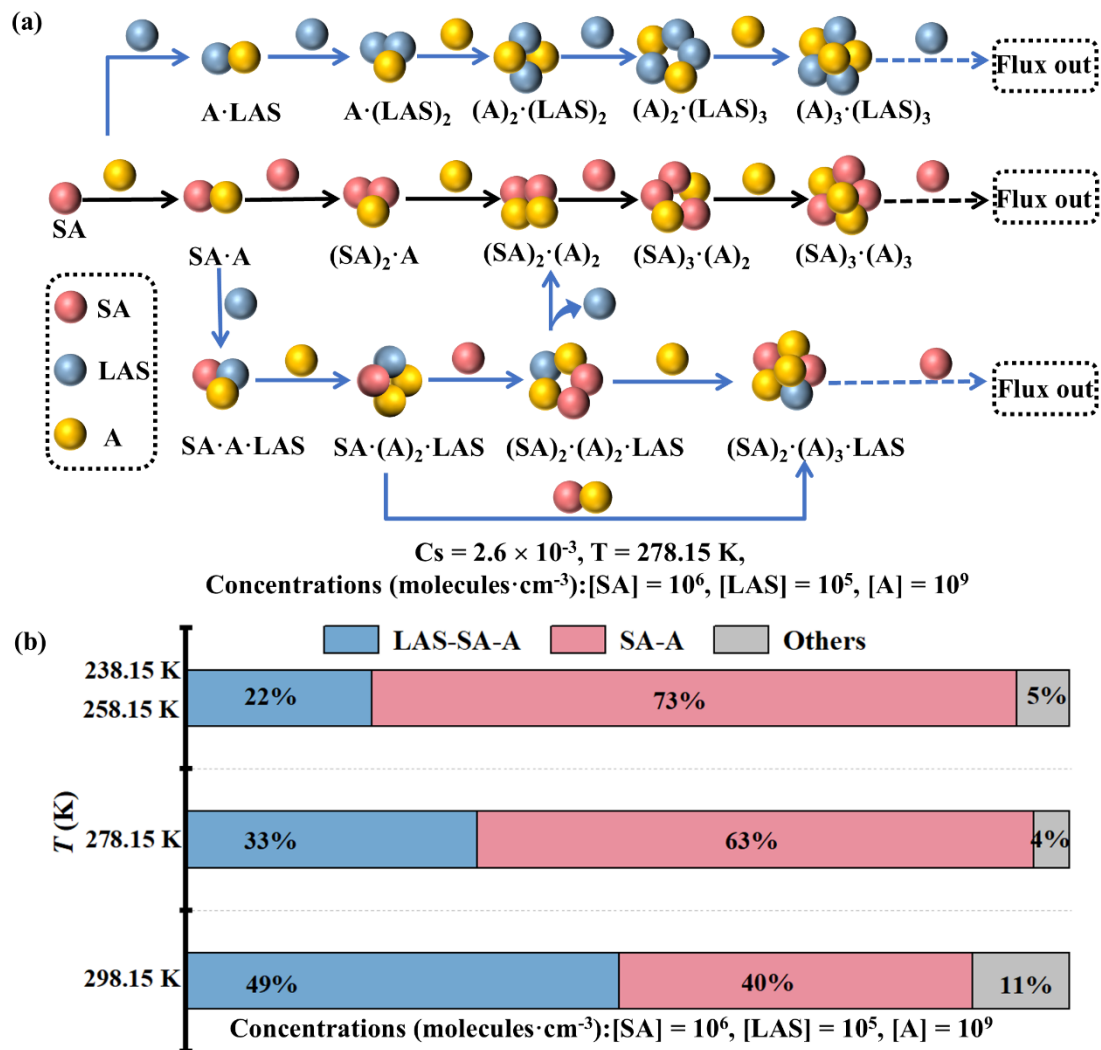


Fig. 5 Nucleation mechanism of the LAS-SA-A system. (a) Cluster formation pathway at 278.15 K, with concentrations of [SA] = 10⁶, [A] = 10⁹ and [LAS] = 10⁵ molecules·cm⁻³; (b) the branch ratio of outward flux at different temperatures. Only net fluxes contributing more than 5% to cluster growth are depicted.

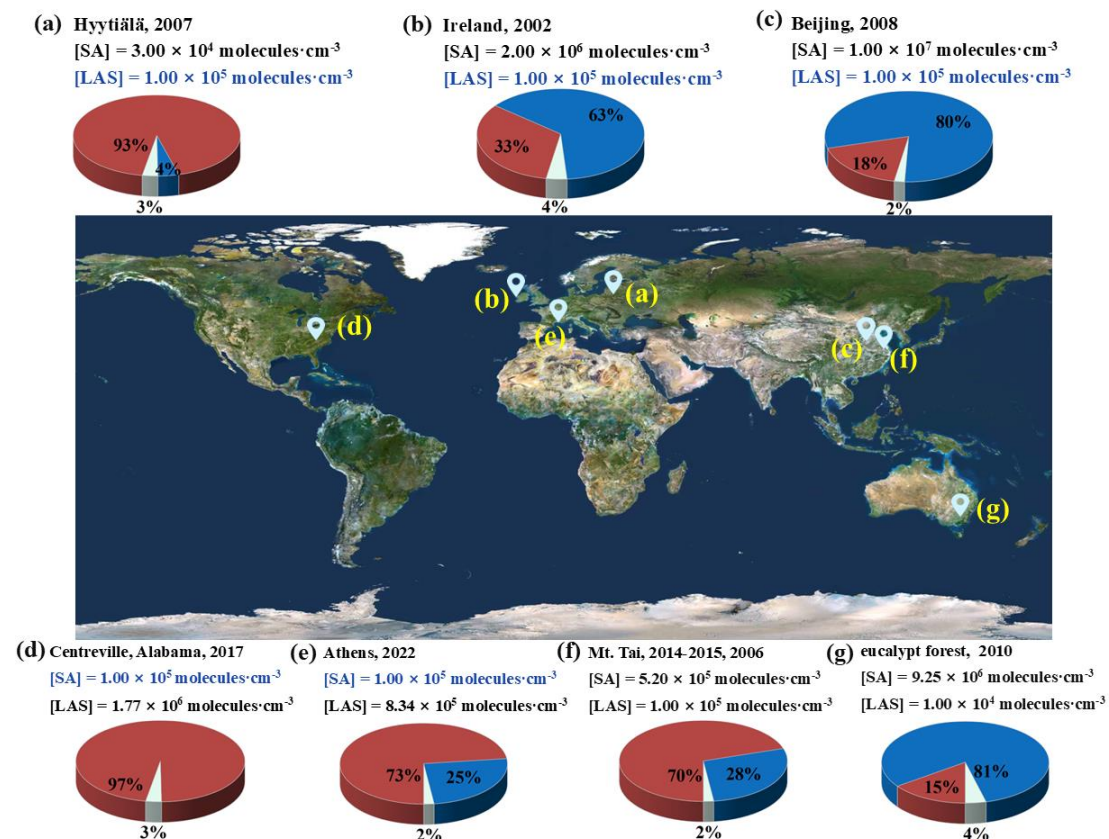


Fig. 6 Branching ratios of SA-A-LAS (red) and SA-A (blue) cluster growth pathways in regions with varying $[LAS]$ concentrations. Black data points indicate field observations, while blue points represent the median values used in this study. Ammonia concentration is fixed at $10^9 \text{ molecules} \cdot \text{cm}^{-3}$. Map source: ©Google Maps (<https://www.google.com/maps>)

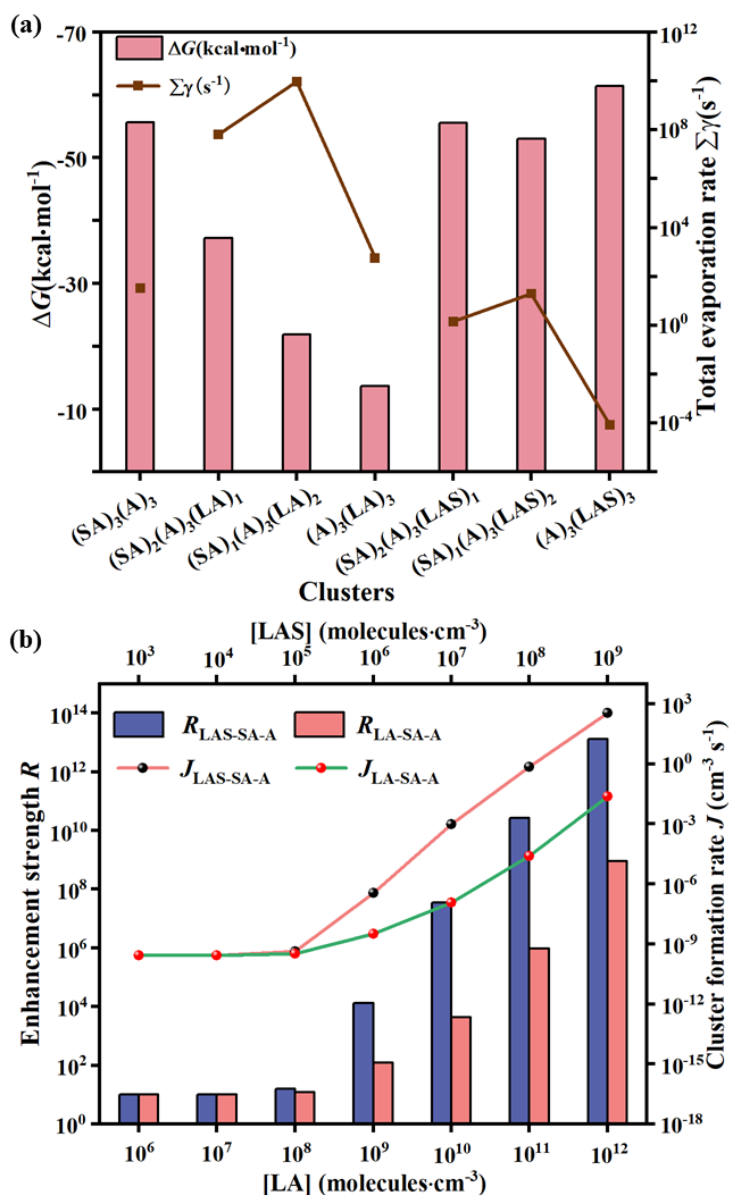


Fig. 7 (a) Gibbs free energies ΔG (kcal·mol⁻¹) and total evaporation rates $\Sigma\gamma$ (s⁻¹) for (LA)_x(SA)_y(A)₃ and (LAS)_x(SA)_y(A)₃ ($x = 0-3$, $x + y = 3$) clusters calculated at the M06-2X/6-311++G(2df, 2pd) level of theory and 278.15 K, (b) Cluster formation rate (J) and enhancement strength (R) for LAS as a function of monomer concentrations ([LA] and [LAS]) at 278.15 K, with [SA] fixed at 10⁵ molecules·cm⁻³ and [A] at 10⁹ molecules·cm⁻³.